THE JOURNAL OF BIOLOGICAL CHEMISTRY
Vol. 275, No. 52, Issue of December 29, pp. 41156–41165, 2000

Printed in U.S.A.

Identification of Domain-Domain Docking Sites within *Clostridium symbiosum* Pyruvate Phosphate Dikinase by Amino Acid Replacement*[S]

Received for publication, July 12, 2000, and in revised form, September 5, 2000
Published, JBC Papers in Press, September 19, 2000, DOI 10.1074/jbc.M006149200

Min Wei‡, Zhong Li§, Dongmei Ye‡, Osnat Herzberg§¶, and Debra Dunaway-Mariano‡¶

From the ‡Department of Chemistry, University of New Mexico, Albuquerque, New Mexico 87131 and the §Center for Advanced Research in Biotechnology, Rockville, Maryland 20850

Potential domain-domain docking residues, identified from the x-ray structure of the *Clostridium symbiosum* apoPPDK, were replaced by site-directed mutagenesis. The steady-state and transient kinetic properties of the mutant enzymes were determined as a way of evaluating docking efficiency. PPDK mutants, in which one of two stringently conserved docking residues located on the N-terminal domain (Arg^{219} and Glu^{271}) was substituted, displayed largely unimpeded catalysis of the phosphoenolpyruvate partial reaction at the C-terminal domain, but significantly impaired catalysis (>10^4) of the ATP pyrophosphorylation of His^{455} at the N-terminal domain. In contrast, alanine mutants of two potential docking residues located on the N-terminal domain (Ser^{262} and Lys^{149}), which are not conserved among the PPDKs, exhibited essentially normal catalytic turnover. Arg^{219} and Glu^{271} were thus proposed to play an important role in guiding the central domain and, hence, the catalytic His^{455} into position for catalysis. Substitution of central domain residues Glu^{434}/Glu^{437} and Thr^{453}, the respective docking partners of Arg^{219} and Glu^{271}, resulted in mutants impaired in catalysis at the ATP active site. The x-ray crystal structure of the apo-T453A PPDK mutant was determined to test for possible misalignment of residues at the N-terminal domain-central domain interface that might result from loss of the Thr^{453}-Glu^{271} binding interaction. With the exception of the mutation site, the structure of T453A PPDK was found to be identical to that of the wild-type enzyme. It is hypothesized that the two Glu^{271} interfacial binding sites that remain in the T453A PPDK mutant, Thr^{453} backbone NH and Met^{452} backbone NH, are sufficient to stabilize the native conformation as observed in the crystalline state but may be less effective in populating the reactive conformation in solution.

Pyruvate phosphate dikinase (PPDK)[1] catalyzes the interconversion of ATP, P_i, and pyruvate with AMP, PP_i, and PEP (1) using two separate active sites linked by a mobile domain containing the phosphoryl group carrier His^{455} (2). At the first active site, to which ATP, P_i and Mg(II) are bound, His^{455} attacks the β-P of ATP, forming a pyrophosphorylhistidine enzyme intermediate (*E*-PP) and AMP (Scheme 1). The P_i ligand then reacts with the terminal phosphoryl group of *E*-PP to form a phosphorylhistidine intermediate (*E*-P) and PP_i. The phosphorylhistidine of *E*-P then moves to the second active site where pyruvate, Mg(II), and a monovalent cation (K^+ or NH_4^+) are bound. Upon transfer of the phosphoryl group to pyruvate to form the final product PEP, the His^{455} residue returns to the first active site to initiate a new catalytic cycle.

The x-ray crystal structure (2) of the three-domain, 96-kDa subunit of the apo-PPDK homodimer from *Clostridium symbiosum* is represented at the *top* of Fig. 1. A Mg(II) cofactor and the ATP and P_i substrate ligands have been modeled into the structure at the N-terminal "ATP grasp" domain (residues 2–430). The locations of the ligand binding sites (comprising active site 1) within the N-terminal domain are supported by the results from earlier affinity labeling and mutagenesis studies (4, 5). As His^{455} is located in close proximity to active site 1, the PPDK crystal structure, with some local adjustments, corresponds to a conformer competent to catalyze the ATP/P_i partial reaction (Scheme 1). Henceforth, this conformer will be referred to as "conformer 1."

Affinity labeling and mutagenesis studies have shown that the pyruvate ligand binds at a second active site, located on the α/β barrel C-terminal domain (residues 534–874) (6, 7). A model of an enzyme conformer (illustrated at the *bottom* of Fig. 1; henceforth referred to as "conformer 2") judged to be effective in catalysis of the pyruvate partial reaction, was generated from the original structure by transferring the central domain (residues 390–504) from its binding site at the concave surface of the N-terminal domain to the concave surface of the C-terminal domain (2). Mg(II) and PEP were modeled into active site 2 of conformer 2 (2) as pictured in Fig. 1 (*bottom*). In this model, the PEP phosphoryl group is aligned for nucleophilic attack by the catalytic His^{455} residue.

We anticipate that the rotation about the two interdomain linkers (residues 341–389 and 505–533), as required by the conformer 1 ↔ conformer 2 model of Fig. 1, occurs freely in solution, thus allowing the central domain to "swivel" between the two active sites. Full catalytic turnover on the enzyme will

* This work was supported by National Institutes of Health Grant GM 36260 (to D. D. M.) and National Science Foundation Grant DMB9019340 (to O. H.). The costs of publication of this article were defrayed in part by the payment of page charges. This article must therefore be hereby marked "*advertisement*" in accordance with 18 U.S.C. Section 1734 solely to indicate this fact.

[S] The on-line version of this article (available at http://www.jbc.org) contains Supplementary Figure 1, which shows the alignment of 17 known PPDK sequences generated using CLUSTALW program supported by the GCG Wisconsin package.

The atomic coordinates and structure factors (code 1ggo) have been deposited in the Protein Data Bank, Research Collaboratory for Structural Bioinformatics, Rutgers University, New Brunswick, NJ (http://www.rcsb.org/).

¶ To whom correspondence should be addressed Tel.: 505-277-3383; Fax: 505-277-2609; E-mail: dd39@unm.edu.

[1] The abbreviations used are: PPDK, pyruvate phosphate dikinase; AMPPNP, adenylimidodiphosphate; PNP, imidodiphosphate; PEP, phosphoenolpyruvate; NADH, dihydronicotinamide adenine dinucleotide; HPLC, high performance liquid chromatography.

ATP/P_i Partial Reaction at Active Site 1 on N-terminal Domain:

(1) E + ATP + P_i → E · ATP · P_i → E-PP · AMP · P_i

(2) E-PP · AMP · P_i → E-P · AMP · PP_i → EP + AMP + PP_i

Pyruvate Partial Reaction at Active Site 2 on C-terminal Domain:

(3) E-P + pyruvate → E-P · pyruvate → E-P · PEP → E + PEP

SCHEME 1. **The ATP/P_i and pyruvate partial reactions of pyruvate phosphate catalysis (1, 3).**

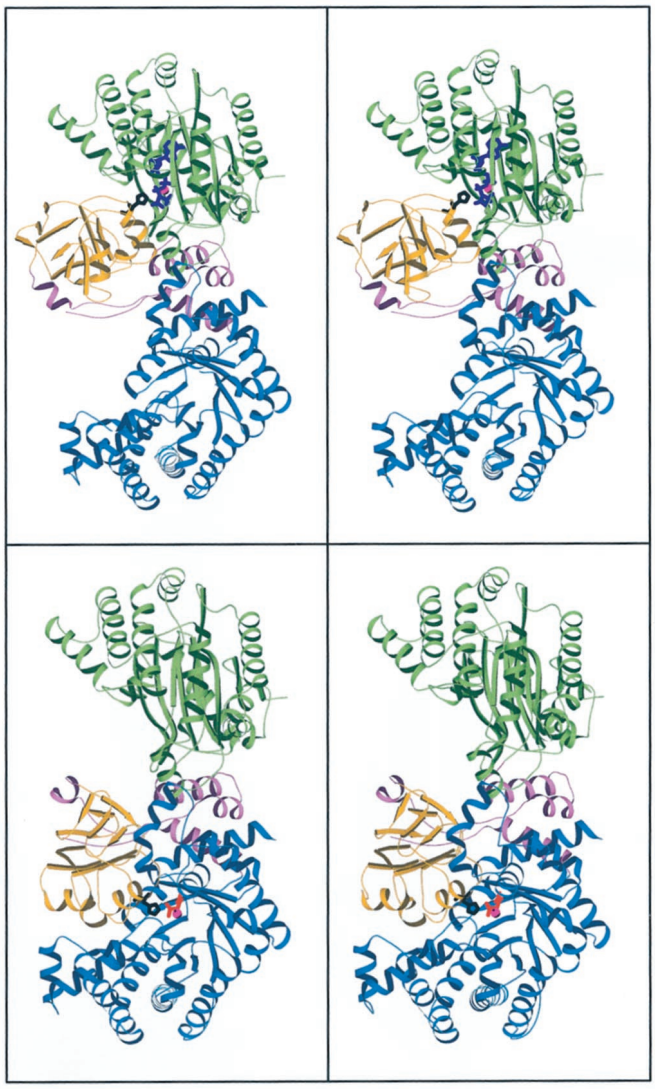

FIG. 1. **MOLSCRIPT stereodiagrams of the *C. symbiosum* PPDK monomer generated from the x-ray coordinates of the apoPPDK structure reported in Ref. 2.** Catalysis of the *E* + ATP + P_i → *E*-P + AMP + PP_i takes place at the N-terminal domain (*green*) active site in conformer 1 (*top structure*; ATP and P_i ligands are *blue*, and Mg(II) is *magenta*), while catalysis of the *E*-P + pyruvate partial reaction takes place at the C-terminal domain (*blue*) active site in conformer 2 (*bottom structure*; PEP ligand is *red*, and Mg(II) is *magenta*). Movement the catalytic His^{455} residue (*black*) between the two active sites is perceived to occur through the interconversion of conformers 1 and 2 via the swivel of the central domain (*yellow*) about its linkers (*pink*).

thus require that ATP, P_i, and Mg(II) first bind to active site 1 of conformer 2 (see Scheme 2). The central domain must then dissociate from the C-terminal domain and bind with the N-terminal domain to form conformer 1. Despite the fact that the rotation about the linkers is intrinsically fast (ns time scale), the central domain must remain docked long enough for catalysis at active site 1 to be completed (millisecond time scale (Ref. 3)), but not so long as to impede the ensuing reaction of $His(P)^{455}$ with pyruvate at active site 2. The transition from conformation 1 to conformation 2 allows dissociation of the AMP and PP_i product ligands from active site 1 as well prepares the enzyme for catalysis at active site 2, provided that this active site was "pre-loaded" with pyruvate and the Mg(II)/NH_4^+ cofactors while the enzyme was in conformation 1. Following catalytic turnover at active site 2 in conformer 2, the central domain must dissociate from the C-terminal domain to allow release of the PEP product from conformer 1. If active site 1 contains ATP and P_i, the next catalytic cycle can directly follow from this conformer.

The separate site catalysis of PPDK thus requires the transient formation of precisely oriented domain-domain complexes. An alignment made of the 17 known PPDK sequences (see Fig. 1 in supplemental materials, available in the on-line version of the journal) shows that a majority of the residues defining the proposed binding surfaces on the N- and C-terminal domains are stringently conserved as are many of the surface residues surrounding the catalytic His^{455} on the central domain (see Fig. 2). In contrast, the surface residues on the opposite, solvent-exposed faces of the three domains are variable. The conservation of residues at the respective domain-domain interfaces of the observed and modeled conformers has been necessary throughout evolution for productive domain docking and accurate targeting of the catalytic His^{455}.

Through inspection of the domain-domain interface region of the x-ray structure of apo-PPDK and of the alignment made of the PPDK sequences, two stringently conserved residues of the N-terminal domain (namely Arg^{219} and Glu^{271}), whose side chains are positioned for favorable polar interaction with side chain and/or backbone atoms of the central domain, were identified. As is shown in Fig. 3, the guanidinium group of Arg^{219} is within interaction distance of the carboxylate groups of the central domain residues Glu^{434} (Glu or Asp conserved) and Glu^{437} (not conserved). The carboxylate group of Glu^{271} is within interaction distance of the hydroxyl group of the central domain Thr^{453} and the backbone amide NHs of Thr^{453} and Met^{452}. In addition, N-terminal domain residues Ser^{262} and Lys^{149}, which are not conserved among all of the PPDK sequences, are also positioned for favorable interaction with the central domain. The hydroxyl group of Ser^{262} is within H-bonding distance of the backbone C=O of central domain residue Ala^{398}. The side-chain ammonium group of Lys^{149} is located 4.4 Å from the central domain Glu^{430} carboxylate, which is too far for significant interaction. However, if the side chain of the Lys^{149} is free to rotate from the conformation observed in the crystal, it can move within 3.5 Å of the carboxylate, close enough for favorable interaction to occur.

Since productive domain-domain binding is an integral component of PPDK catalysis (Scheme 2), an examination of the roles of Arg^{219}, Glu^{271}, Ser^{262}, and Lys^{149} in domain docking can be made by replacing these residues with amino acids that can not interact favorably and evaluating the catalytic efficiencies of the corresponding mutant enzymes. In the text that follows, we report on the steady-state and transient kinetic properties of the *C. symbiosum* PPDK mutants R219A, R219E, E434A/E437A, E271A, T453A, S262A, S262W, and K149A. The rate constants obtained for the mutants in catalysis of the full reaction and the *E* + ATP → *E*-PP·AMP, *E* + ATP + P_i → *E*-P·AMP·PP_i, and *E* + PEP → *E*-P·pyruvate partial reactions are compared with those determined in an earlier kinetic analysis of the wild-type PPDK (8). The results suggest that the productive docking of the central domain is controlled, in part, through the interaction of N-terminal domain residues Arg^{219}

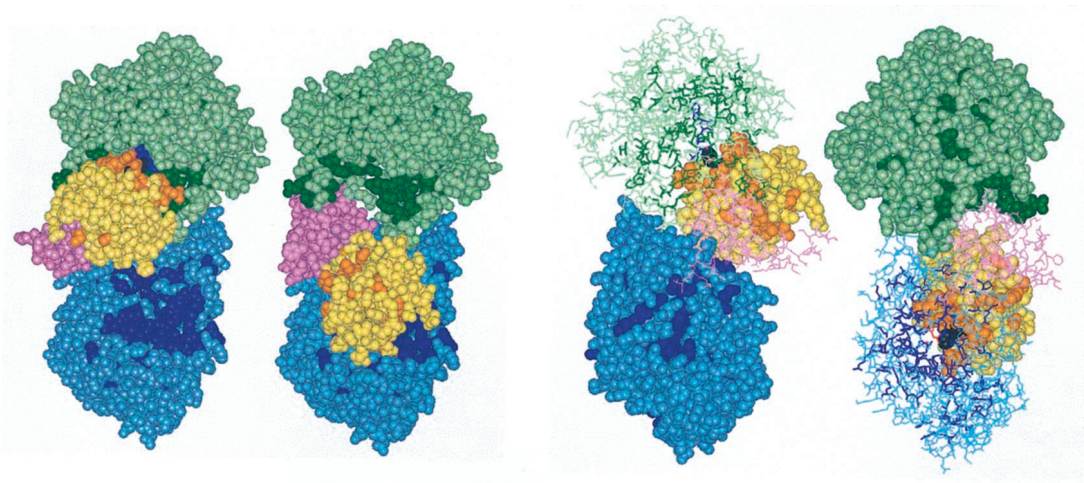

FIG. 2. **Front and back views of the space filling models of the PPDK conformers 1 and 2 of Fig. 1 are shown to illustrate the conservation of residues at the domain-domain interface regions.** The *dark green*, *dark blue*, and *gold* residues are stringently conserved among the 17 known PPDK sequences, while the *pastel blue*, *pastel green*, and *yellow* residues are variable.

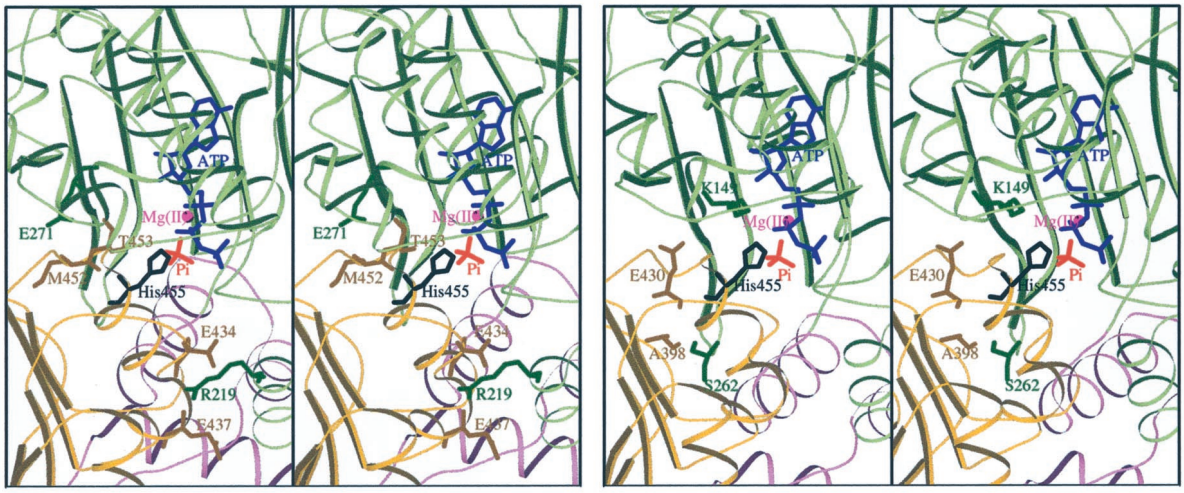

FIG. 3. **A stereoview of the Arg^{219}-Glu^{434}/Glu^{437} and Glu^{271}-Met^{452}/Thr^{453} docking sites (*a*) and the Ser^{262}-Ala^{398} and Lys^{149}-Glu^{430} interactions at the interface of the N-terminal and central domains (*b*).** The N-terminal domain interface is shown in *green*, the central domain interface in *yellow*, and the domain linkers in *pink*. The ATP ligand is *blue*, the P_i ligand *red*, the Mg(II) ion is *magenta*, and the catalytic His^{455} is *black*.

and Glu^{271} with central domain residues Glu^{434}/Glu^{437} and Thr^{453}/Met^{452}, respectively. The N-terminal domain Ser^{262} and Lys^{149} residues, on the other hand, do not appear to play a vital role in orienting or stabilizing the domain-domain complex.

EXPERIMENTAL PROCEDURES

Preparation of C. symbiosum PPDK Mutants—Mutant genes were prepared from the plasmid pACYC184-D12 (9) using polymerase chain reaction techniques analogous to those described in (4). Mutagenic primers, 18–22 base pairs in length, were synthesized by Life Technologies, Inc. *Bgl*II and *Bst*XI restriction sites were employed in the construction of the Lys^{149}, Arg^{219}, Ser^{262}, and Glu^{271} mutants, whereas *Bst*XI and *Kpn*I sites were used for the Glu^{434}/Glu^{437} and Thr^{453} mutants. The sequences of the isolated mutant genes were determined at the Center for Agricultural Biotechnology at the University of Maryland. Wild-type and mutant PPDK genes were expressed in *Escherichia coli* JM101 cells, and the protein products were purified to homogeneity (judged by SDS-polyacrylamide gel electrophoresis analysis) in yields of 20–25 mg/g cell as described in Ref. 4. The chromatographic properties of the mutant proteins as well as their stability to storage in buffered solutions at 4 °C were observed to be very similar to the chromatographic properties and stability of the wild-type enzyme.

Steady-state Kinetic Analysis—The spectrophotometric assay described in Ref. 10 was used to monitor the initial velocity of the PPDK-catalyzed reaction of AMP, PP_i, and PEP to ATP, P_i, and pyruvate. Initial velocities were measured as a function of the concentration of the varied substrate (in a range of 0.5–10-fold K_m) at fixed, saturating concentrations of cosubstrates (0.5 mM AMP, 0.5 mM PEP, 1 mM PP_i) and metal ion cofactors (5 mM $MgCl_2$ and 40 mM NH_4Cl) in 20 mM imidazole (pH 6.8, 25 °C). The initial velocity data were analyzed using Equation 1 and the computer programs of Cleland (11). The k_{cat} was calculated from $v_{max}/[E]$.

$$v_0 = v_{max}\,[S]/(K_m + [S]) \qquad \text{(Eq. 1)}$$

v_0 is the initial velocity, $[E]$ is the enzyme concentration, [S] is the substrate concentration, v_{max} is the maximum velocity, and K_m is the Michaelis constant. The K_i values for the competitive inhibitors AMP-PNP and PNP were determined from initial velocity data obtained at varying AMP or PP_i concentrations and fixed, saturating concentrations of cosubstrates and cofactors. The initial velocity data were analyzed using Equation 2, where K_i is the inhibition constant and [I] the inhibitor concentration.

$$v_0 = v_{max}\,[S]/[K_m(1 + [I]/K_i) + [S]] \qquad \text{(Eq. 2)}$$

Rapid Quench Analysis of PPDK-catalyzed Single-turnover Reactions of [^{32}P]PEP—[^{32}P]PEP was prepared from [β-^{32}P]ATP according to the procedure described in Carroll *et al.* (3). [β-^{32}P]ATP (specific activity >

TABLE I

Steady-state kinetic constants for wild-type and mutant PPDK catalysis of AMP + PP_i + PEP → ATP + P_i + pyruvate in 20 mM imidazole-HCl (pH 6.8) containing 40 mM NH_4Cl and 5 mM $MgCl_2$ at 25 °C

Sample	K_m	k_{cat}	K_i
	mM	s^{-1}	*mM*
Wild-type (0.006–0.02 μM)			
Vary AMP[a]	0.009 ± 0.002	22 ± 2	0.07 ± 0.01 (AMPPNP)
Vary PP_i[b]	0.088 ± 0.005	28 ± 1	0.031 ± 0.02 (PNP)
Vary PEP[c]	0.027 ± 0.0005	25 ± 1	
R219E (0.045–0.21 μM)			
Vary AMP[a]	0.010 ± 0.002	3.2 ± 0.2	0.09 ± 0.01 (AMPPNP)
Vary PP_i[b]	0.22 ± 0.01	3.8 ± 0.2	0.71 ± 0.06 (PNP)
Vary PEP[c]	0.0055 ± 0.0003	4.2 ± 0.5	
R219A (0.053–0.21 μM)			
Vary AMP[a]	0.0044 ± 0.005	1.83 ± 0.06	0.08 ± 0.01 (AMPPNP)
Vary PP_i[b]	0.158 ± 0.006	2.8 ± 0.1	>3 (PNP)
Vary PEP[c]	0.010 ± 0.001	2.14 ± 0.04	
E434A/E437A (0.055–0.24 μM)			
Vary AMP[a]	0.004 ± 0.001	2.21 ± 0.02	0.03 ± 0.01 (AMPPNP)
Vary PP_i[b]	0.091 ± 0.004	2.72 ± 0.06	>4 (PNP)
Vary PEP[c]	0.0048 ± 0.0003	2.64 ± 0.05	
E271A (10 μM)		< 0.005	
T453A (0.11–0.42 μM)			
Vary AMP[a]	0.0029 ± 0.0002	1.14 ± 0.02	0.11 ± 0.01 (AMPPNP)
Vary PP_i[b]	0.078 ± 0.002	1.52 ± 0.02	>4 (PNP)
Vary PEP[c]	0.0044 ± 0.0002	1.34 ± 0.02	
S262A (0.004–0.017 μM)			
Vary AMP[a]	0.0033 ± 0.0002	21 ± 1	0.11 ± 0.01 (AMPPNP)
Vary PP_i[b]	0.067 ± 0.005	25 ± 1	0.03 ± 0.002 (PNP)
Vary PEP[c]	0.0037 ± 0.0002	20 ± 1	
S262W (1.2–2.3 μM)			
Vary AMP[a]	0.0075 ± 0.0003	0.15 ± 0.01	0.32 ± 0.02 (AMPPNP)
Vary PP_i[b]	0.187 ± 0.006	0.27 ± 1	>4 (PNP)
Vary PEP[c]	0.002 ± 0.0003	0.45 ± 0.03	
K149A (0.013–0.031 μM)			
Vary AMP[a]	0.0103 ± 0.0008	14.4 ± 0.6	0.30 ± 0.01 (AMPPNP)
Vary PP_i[b]	0.082 ± 0.005	15.6 ± 0.5	0.011 ± 0.006 (PNP)
Vary PEP[c]	0.0043 ± 0.0003	15.4 ± 0.8	

[a] Reactions contained 1.0 mM PP_i, 0.5 mM PEP.
[b] Reactions contained 0.5 mM AMP, 0.5 mM PEP.
[c] Reactions contained 1.0 mM PP_i, 0.5 mM AMP.

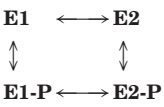

E2 binds & releases ATP, P_i pair or AMP, PP_i pair but reacts only with bound PEP

E2-P binds & releases ATP, P_i pair or AMP, PP_i pair but reacts only with bound pyruvate

E1 binds & releases pyruvate or PEP but reacts only with bound ATP, P_i pair

E1-P binds & releases pyruvate or PEP but reacts only with bound AMP, PP_i pair

SCHEME 2. **An illustration of the free and phosphorylated forms of PPDK conformer 1 (E_1, E_1-P) and conformer 2 (E_2, E_2-P) (see Fig. 1) with the ligands that these enzyme forms bind and convert to products.**

1 Ci/mmol) was custom-synthesized by PerkinElmer Life Sciences. The single-turnover reactions of 40 μM wild-type or mutant PPDK, 5 μM [^{32}P]PEP, 2.5 mM $MgCl_2$, and 10 mM NH_4Cl in 50 mM K^+Hepes (pH 7.0, 25 °C) were carried out in a rapid quench apparatus from KinTek Instruments. Reactions were initiated by mixing 32 μl of buffered enzyme/cofactors with 32 μl of buffered substrate and then terminated at varying conversion with 182 μl of 0.6 M HCl. The protein was precipitated from quenched solutions by vigorous mixing with CCl_4 and separated by centrifugation. The protein pellet (dissolved in 500 μl of boiling 10 N H_2SO_4) and supernatant were analyzed for ^{32}P by scintillation counting. The percentage of conversion was deduced from the ratio of the radioactivity in the pellet to the total radioactivity in the pellet and supernatant. The concentration of [β-^{32}P]*E*-P was calculated from 40 μM *X*% conversion and plotted as a function of reaction time. The resulting time course was fit to a single exponential equation (Equation 3) using the KaleidaGraph computer program to yield the reported rate constants.

$$[B]_t = [B]_f \times (1 - \exp(k_{obs} \times t)) \quad \text{(Eq. 3)}$$

$[B]_t$ is the product concentration at time *t*, $[B]_f$ is the product concentration at equilibrium, and k_{obs} is the observed rate constant for the reaction.

Rapid Quench Analysis of PPDK-catalyzed Single-turnover Reactions of [^{14}C]ATP in the Absence or Presence of P_i—[^{14}C]ATP was synthesized from [^{14}C]AMP (PerkinElmer Life Sciences) as follows. A 1-ml reaction containing 0.08 μM [^{14}C]AMP (50 μCi), 50 μM PP_i, 0.5 mM PEP, 5 mM $MgCl_2$, 40 mM NH_4Cl, 6 units of PPDK in 50 mM K^+Hepes (pH 7.0) was carried out at 25 °C for 1 h. The reaction mixture was then chromatographed on a 9-ml DEAE-Sepharose column using a linear gradient (0.25–1.1 M) of triethylamine bicarbonate (pH 7) as eluant. The fractions containing [^{14}C]ATP were pooled and concentrated *in vacuo* (rotary evaporation) at room temperature. Excess triethylamine bicarbonate was removed by repeated water dilution followed by evaporation. The resulting [^{14}C]ATP was stored frozen in 50 mM K^+Hepes buffer (pH 7.0) at −30 °C.

Single-turnover reactions of 40 μM wild-type or mutant PPDK, 10 μM [^{14}C]ATP, 2.5 mM $CoCl_2$, and 10 mM NH_4Cl in 50 mM K^+Hepes (pH 7.0, 25 °C) were carried out in the presence or absence of 11 mM P_i using a rapid quench device as described previously. The protein was removed from the acid quenched samples by centrifugation through a 500-μl filter (cut-off molecular mass of 30 kDa) purchased from Pall Gelman Inc. The unconsumed [^{14}C]ATP and [^{14}C]AMP product were separated by HPLC using a Beckman ultrasphere C18 reversed-phase analytical column and 25 mM KH_2PO_4, 2.5% triethylamine, and 5% methanol as the mobile phase. The fractions containing ATP and AMP were analyzed for ^{14}C content by liquid scintillation counting. The time course for a single-turnover reaction was constructed, and the k_{obs} was calculated, in the manner described in the previous section.

X-ray Crystallographic Analysis of T453A PPDK—The crystallization conditions used for the *C. symbiosum* T453A PPDK mutant were the same as those used for the wild-type enzyme (2). Single crystals

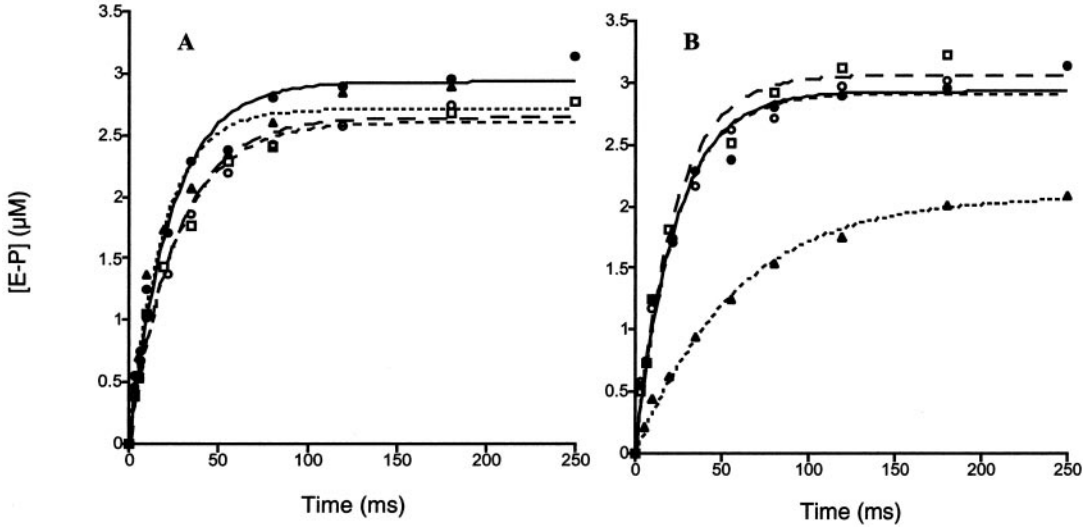

FIG. 4. **The time courses for [^{32}P]*E*-P formation in the single-turnover reaction of 40 μM wild-type or mutant PPDK, 5 μM [^{32}P]PEP, 2.5 mM $MgCl_2$, and 10 mM NH_4Cl in 50 mM K^+Hepes (pH 7.0, 25 °C).** *A*, wild-type (●), R219A (○), R219E (□), and E434A/E437A (▲). *B*, wild-type (●), E271A (○), S262W (□), and T453A (▲). The curves were generated by computer fitting the data to a first order rate equation using the computer program KaleidaGraph. The k_{obs} values calculated from these curves are reported in Table II.

TABLE II

The single-turnover rate constants measured wild-type, R219E, R219A, E434A/E437A, E271A, T453A, and S262W catalysis of the E + [^{32}P]PEP → [^{32}P]E-P · pyruvate partial reaction

Single-turnover reactions contained 40 μM enzyme, 5 μM [^{32}P]PEP, 2.5 mM $MgCl_2$, and 10 mM NH_4Cl in 50 mM K^+Hepes (pH 7.0, 25 °C). See "Experimental Procedures" for details.

Enzyme	k_{obs}
	s^{-1}
Wild-type	43 ± 4
R219E	38 ± 4
R219A	38 ± 4
E271A	49 ± 4
E434A/E437A	52 ± 6
T453A	17 ± 1

were obtained at 30 °C by vapor diffusion in hanging drops. Protein drops were equilibrated against reservoir solutions containing 50–55% saturated ammonium sulfate and 100 mM Hepes buffer (pH 7.0). The drops consisted of protein solution (10 mg/ml, 20 mM imidazole buffer (pH 6.5), 100 mM KCl, 0.1 mM EDTA, and 1 mM mercaptoethanol), diluted by an equal volume of reservoir solution. The crystals belong to space group P_2, and within the accuracy of the data the unit cell dimensions are the same as those of the wild-type protein crystals (Table II). The crystal was transferred to a mother liquor solution containing 20% glycerol, and then flash-frozen using an Oxford cryosystem. X-ray diffraction data were collected on a Siemans area detector mounted on a three-circle goniostat, with a monochromated CuK_α x-ray supplied by a Rigaku Rotaflex RU200BH rotating anode generator. Data were processed with the XENGEN package (12). Data collection statistics are provided in Table VI. Structure refinement was performed with the program CNS (13). The simulated annealing slow-cooling protocol at 3000 K was followed by positional and temperature factor refinement cycles. Data up to 2.65 Å for which $F \geq 2\sigma(F)$ were included. Adjustments to the model were made on a Silicon Graphics INDIGO II computer graphics workstation using the program TURBO-FRODO (14).

RESULTS AND DISCUSSION

Steady-state Kinetic Properties of PPDK Mutants—The PPDK mutants were first screened by measuring k_{cat} and K_m values for substrates and K_i values for competitive inhibitors. The steady-state kinetic constants were determined for the AMP + PP_i + PEP → ATP + P_i + pyruvate reaction (with Mg^{2+} and NH_4^+ serving as cofactors) using a continuous spectrophotometric assay to monitor pyruvate formation. PPDK adheres to an ordered, nonclassical bi (ATP, P_i) bi (PP_i, AMP) uni (pyruvate) uni (PEP) kinetic mechanism (10). For convenience, the K_m (and V_m) for each substrate was evaluated from initial velocity data measured with the concentrations of the two co-substrates held constant at saturating levels, while the concentration of the third substrate was varied at ~0.5–10-fold the K_m value. The K_i values of the ATP analog AMPPNP (*versus* AMP) and PP_i analog PNP (*versus* PP_i) were determined from the initial velocity data measured in the absence and presence of the inhibitor.

The K_i, K_m, and k_{cat} values obtained for wild-type PPDK and the PPDK mutants at pH 6.8 and 25 °C are listed in Table I. Except for S262A and K149A, each of the mutants display significantly reduced catalytic efficiency compared with that of the wild-type PPDK. The k_{cat} is deceased ~10-fold for the R219A, R219E, and E434A/E437A mutants, ~20-fold for T453A, ~100-fold for S262W, and >5000-fold for E271A. As will be described in the section that follows, the reduction in k_{cat} derives from a reduction in the rate of the nucleotide partial reaction.

The abilities of the mutant enzymes to bind ATP and PP_i are reflected by the K_i values measured for the inert analogs AMPPNP and PNP. AMPPNP competes with AMP for the same binding site on conformer 1 of the free and phosphorylated forms of the enzyme (see Scheme 2). Likewise, PNP competes with PP_i for the same site on the AMP complex of the free or phosphorylated enzyme in conformation 1. An increase in the K_i value may signify that the structure or electronic environment of the binding site has been altered by the mutation. Alternatively, if the ligand binding site is changed by domain-domain association, a mutation that affects domain binding can affect the K_i of the inhibitor. Thus, an increase in the K_i values may also indicate impaired domain-domain docking.

Based on the AMPPNP K_i values listed Table I, it is evident that the ATP binding affinity is not altered in the R219E, R219A, E343A/E347A, S262A, and T453A mutants, despite the fact that all but the S262A mutant has a significantly lower turnover rate. On the other hand, the AMPPNP K_i values measured for the S262W and K149A mutants are ~4-fold larger than that measured for wild-type PPDK. The exact cause of reduced ATP binding in these mutants is presently unknown; however, since the Ser^{262} and Lys^{149} residues do not appear to function as docking residues (*i.e.*, the k_{cat} values of the Ala mutants are normal), we have not pursued the issue further.

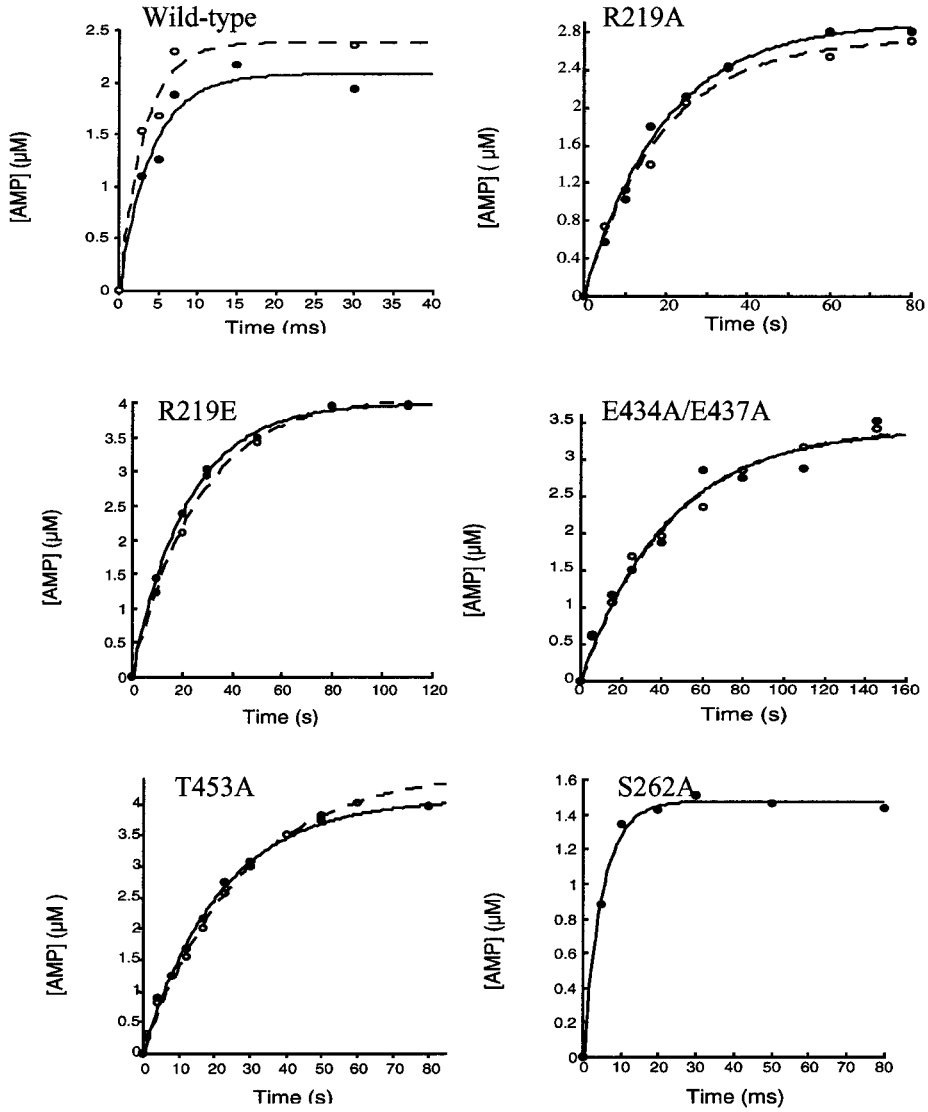

FIG. 5. **The time courses for [^{14}C]AMP formation in the single-turnover reactions of 40 μM (●) or 80 μM (○) enzyme, 10 μM [^{14}C]ATP, 5 mM $MgCl_2$, and 10 mM NH_4Cl in 50 mM K^+Hepes (pH 7.0, 25 °C) catalyzed by wild-type, R219E, R219A, E434A/E437A, T453A, and S262A PPDK.** The plots are generated by fitting the time point data to a first order rate equation.

The PP_i binding affinity was found to be severely weakened in the R219E, R219A, E434A/E437A, S262W, and T453A PPDK mutants, as indicated by the comparatively large PNP K_i values observed for the mutant enzymes (~20–100-fold larger than that of the wild-type PPDK). Only the K149A and S262A mutants, both of which display normal k_{cat} values (and thus, unimpaired domain-domain docking), were unaffected. The PP_i binding site lies outside of the regions mutated and, therefore, may not be directly effected by the amino acid replacements made. On the other hand, PP_i binds at the entrance of active site 1, which becomes desolvated by the region of the central domain surrounding (and including) the His(P)^{455}. A likely scenario is that the reduced PNP binding affinity observed with the mutant enzymes is a reflection of altered domain-domain binding.[2]

Catalysis at the PEP/Pyruvate Active Site—The *E*·PEP ′ *E*-P·pyruvate partial reaction is catalyzed by PPDK in conformation 2 (Fig. 1; Scheme 2). Thus, mutations made at the N-terminal domain are not expected to inhibit catalysis at the C-terminal domain. This was tested by measuring the k_{obs} for single-turnover reactions of R219A, R219E, E271A, and S262W mutant PPDK + [^{32}P]PEP → [^{32}P]*E*-P·pyruvate using rapid quench techniques. The time courses for these reactions are shown in Fig. 4, whereas the k_{obs} values calculated from the rate data are reported in Table II. All four mutants displayed normal catalysis of the *E*·PEP ↔ *E*-P·pyruvate partial reaction. The fact that the k_{obs} values for the four mutants are not noticeably higher than that measured for the wild-type enzyme suggests that the population of conformer 2 has not been significantly increased and/or that the rate of conformer equilibration is not limiting.

[2] In contrast to the ATP binding site, the P_i binding site is located at the entrance to the active site crevice where Arg337, and possibly Mg(II), are the probable binding residues (4) D. Ye, M. Wei, M. V. McGuire, K. Huang, G. Kapadia, O. Herzberg, and D. Dunaway-Mariano, unpublished data). The affinity of P_i for this site is quite low (K_d ~ 6 mM) and the binding rate, slow (k_{on} = 0.04 μM^{-1} s^{-1}; k_{off} ~200 s^{-1}) (8). Since ATP binds beneath the P_i, substrate binding is ordered, with ATP first and P_i second (10). When the central domain binds to the N-terminal domain, the active site is closed and the dissociation of the two substrate ligands is prevented. The P_i ligand is covered by the central domain region surrounding the catalytic His^{455} (see Fig. 1). Whether or not direct binding interaction occurs between the bound P_i ligand and the central domain, cannot be discerned on the basis of the data on hand. Nevertheless, it is reasonable to expect that the domain docking produces significant alterations in the P_i environment. The PP_i ligand displays a higher binding affinity for the *E*-P·AMP complex (K_d = 50 μM) than does P_i for the enzyme-ATP complex (8, 10). PP_i binding (k_{on} = 2 μM^{-1} s^{-1}; k_{off} = 100 s^{-1} (Ref. 8)) is followed by phosphohistidine 455 binding. It is likely that the environment of the PP_i ligand is altered by domain-domain association and that the PP_i binding constant is effected by mutations that impair the domain-domain docking reaction.

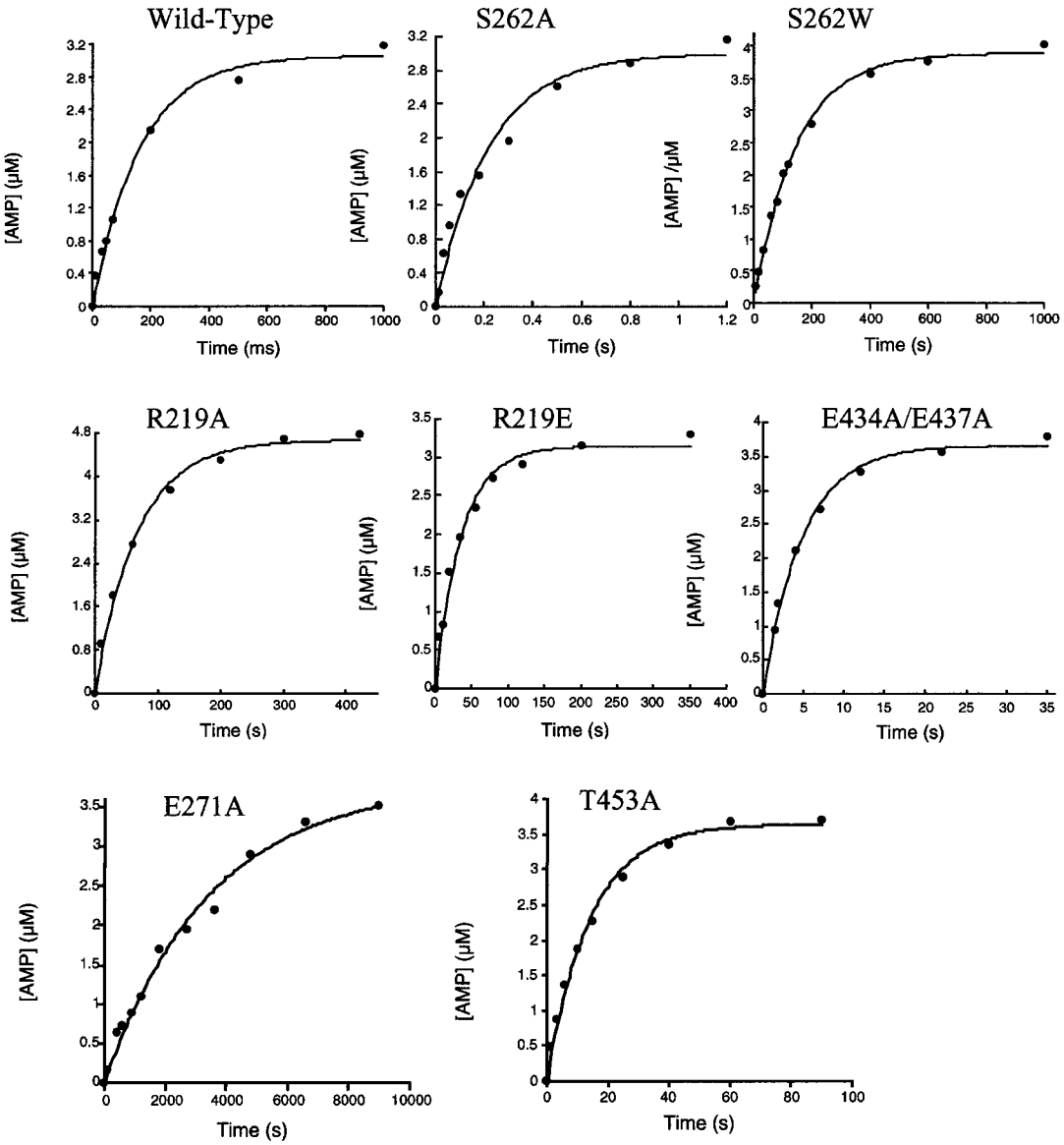

FIG. 6. **The time courses for [^{14}C]AMP formation in the single-turnover reactions of 5 μM [^{14}C]ATP, 11 mM P_i, 5 mM $MgCl_2$, and 10 mM NH_4Cl in 50 mM K^+Hepes (pH 7.0, 25 °C) catalyzed by 20 μM enzyme wild-type, R219E, R219A, E434A/E437A, E271A, T453A, S262A, and S262W PPDK.** The plots are generated by fitting the time point data to a first order rate equation.

The E434A/E437A and T453A mutations modify the central domain. Since the central domain must interface with the C-terminal domain in order to catalyze the *E*·PEP ↔ *E*-P·pyruvate partial reaction, it was anticipated that the central domain mutants would display reduced catalytic efficiency at both active sites. However, the time course measured for the *E* + [^{32}P]PEP → [^{32}P]*E*-P·pyruvate single-turnover catalyzed by the E434A/E437A mutant is essentially the same as that catalyzed by wild-type PPDK, whereas that measured for the T453A mutant reflects ~2-fold reduction in k_{obs} and ~30% reduction in the position of the reaction equilibrium ([*E*-P] [pyruvate] [*E*-P·pyruvate]/[*E*] [PEP] [*E*·PEP], where for wild-type PPDK the K_d values for *E*-P·pyruvate and *E*·PEP complexes are 75 and 170 μM, respectively, and the internal K_{eq} = [*E*-P·pyruvate]/[*E*·PEP] = 1 (Ref. 8)) (Fig. 4; Table II). The Glu^{434} and Glu^{437} residues of the central domain thus do not appear to function as docking sites in the association of the central and C-terminal domains. On the other hand, the Thr^{453} residue appears to play a minor role in promoting catalysis at the C-terminal active site.

Catalysis at the ATP/P_i Active Site—Catalysis at the N-terminal domain consists of two reaction steps: the pyrophosphorylation of His^{455} by ATP, followed by the transfer of a phosphoryl group from the pyrophosphorylated His^{455} to phosphate (see Scheme 1). Both reaction steps require activation of the enzyme by a divalent metal ion (Mg(II) is the physiological cofactor, but Co(II) and Mn(II) are also effective activators) (1).

The reaction of His^{455} with ATP does not require P_i and, thus, can be studied in isolation. The single-turnover reaction of excess PPDK with [^{14}C]ATP to produce *E*-PP·[^{14}C]AMP is monitored using a rapid quench instrument in conjunction with HPLC techniques to separate the [^{14}C]AMP released from the quenched enzyme (8). Previous studies of the wild-type PPDK have shown that the amount of AMP formed under the conditions of the single-turnover reaction is governed by the level of enzyme-bound *versus* unbound ATP and by the [*E*-PP·AMP]/[*E*·ATP] equilibrium (8). Substitution of Co(II) for Mg(II) as cofactor in the reaction increases both ATP binding to the enzyme and the internal equilibrium, so that the amount of *E*-PP·AMP produced from reaction of 40 μM PPDK with 10 μM ATP increases from ~5% for the Mg(II)-activated enzyme to ~25% for the Co(II)-activated enzyme. For this reason, the

TABLE III

Single-turnover rate constants for wild-type, R219E, R219A, E434A/E437A, E271A, T453A, S262A, and S262W PPDK catalysis of E + [^{14}C]ATP → E-PP · [^{14}C]AMP

Reaction contains 40 μM enzyme, 10 μM [^{14}C]ATP, 2.5 mM Co^{2+}, 10 mM NH_4^+, and 50 mM K^+Hepes (pH 7.0, 25 °C).

Enzyme	k_{obs}
	s^{-1}
Wild-type	~300 ± 70[a]
R219E	0.03 ± 0.03[b]
R219A	0.050 ± 0.004[b]
E434A/E437A	0.08 ± 0.05[b]
E271A	<0.005[c]
T453A	0.046 ± 0.003
S262A	200 ± 20
S262W	≤0.005[c]

[a] Average results of two reaction trials carried out using separately prepared enzymes. The marked error was the difference between the k_{obs} values obtained from the two trials.

[b] The wild-type PPDK catalyzed ATP reaction reached more than 60% conversion within the dead time of the rapid quench instrument; therefore, the wild-type k_{obs} was only an estimated value.

[c] Mutant E271A- and S262W-catalyzed ATP turnover reactions were too slow to be accurately quantitated due to considerable decomposition of nucleotides at the active sites of these mutants when incubation time exceeded 300 s. The lower limit of measurable rate constant is 0.005 s^{-1}.

TABLE IV

Single-turnover rate constants for wild-type, R219E, R219A, E434A/E437A, E271A, T453A, S262A, and S262W PPDK catalysis of E + [^{14}C]ATP + P_i → E-P + [^{14}C]AMP + PP_i

Single-turnover reaction contains 20 μM enzyme, 5 μM [^{14}C]ATP, 11 mM P_i, 5 mM Mg^{2+}, 10 mM NH_4^+, and 50 mM K^+Hepes (pH 7.0, 25 °C).

Enzyme	k_{obs} for trial 1	k_{obs} for trial 2	k_{obs}
	s^{-1}	s^{-1}	s^{-1}
Wild-type	6.2 ± 0.6	5.7 ± 0.3	6.0 ± 0.6[a]
R219A	0.015 ± 0.001	0.015 ± 0.001	0.015 ± 0.001[a]
R219E	0.014 ± 0.001	0.028 ± 0.002	0.02 ± 0.01[a]
E434A/E437A	0.13 ± 0.01	0.21 ± 0.01	0.17 ± 0.08[a]
E271A			0.00029 ± 0.00003
T453A			0.071 ± 0.005
S262A			4.5 ± 0.6
S262W			0.0069 ± 0.0003

[a] Average results of two reaction trials carried out using separately prepared enzymes. The marked error was the difference between the k_{obs} values obtained from the two trials.

abilities of the PPDK mutants to catalyze the E + [^{14}C]ATP → E-PP·[^{14}C]AMP partial reaction were evaluated using Co(II) rather than Mg(II) as cofactor.

On the other hand, Mg(II) is the superior choice for kinetic analysis of the single-turnover reaction of E (20 μM) + ATP (5 μM) + P_i (11 mM) → E-P·AMP·PP_i. For this reaction, it is advantageous to minimize the level of AMP formed in the initial E·ATP P_i → E-PP·AMP·P_i step so that the total amount of AMP formed will coincide with the amount of AMP produced as the result of the second partial reaction: E-PP·AMP·P_i → E-P·AMP·PP_i, which, by mass action effect, drives the first reaction forward. For wild-type PPDK, the k_{obs} for the first step is ~ 300 s^{-1} while the k_{obs} for the second step is ~6 s^{-1} (4).

If catalysis of the first step is impaired in the PPDK mutant, this will be reflected by the time course for [^{14}C]AMP formation in the E·Co(II) + [^{14}C]ATP → E-PP· [^{14}C]AMP·Co(II) reaction, as well as by the time course for [^{14}C]AMP formation in the E·Mg(II) + [^{14}C]ATP + P_i → E-P·[^{14}C]AMP·PP_i·Mg(II) reaction. If, on the other hand, the first step is not severely inhibited, then the degree to which the second step is inhibited can be discerned from the time course for [^{14}C]AMP formation in the E·Mg(II) + [^{14}C]ATP + P_i → E-PP·[^{14}C]AMP·PP_i·Mg(II) reaction (see for example, Ref. 4).

The time courses for [^{14}C]AMP formation in the E·Co(II) + [^{14}C]ATP → E-PP·[^{14}C]AMP·Co(II) reaction and in the E·Mg(II) + [^{14}C]ATP + P_i → E-P·[^{14}C]AMP·PP_i·Mg(II) reaction catalyzed by wild-type and mutant PPDK are shown in Figs. 5 and 6, whereas the observed rate constants calculated from the rate data are listed in Tables III and IV. S262A mutant catalyzes the E·Co(II) + [^{14}C]ATP → E-PP· [^{14}C]AMP·Co(II) reaction at the normal (wild-type) rate, while the rates observed for the R219E, R219A, E434A/E437A, E271A, T453A, and S262W mutants are drastically lower (10^4 to $>10^5$). The k_{obs} was remeasured using double the concentration of mutant or wild-type PPDK to determine whether E·Co(II)· [^{14}C]ATP complex formation or catalytic turnover is rate-limiting in the single-turnover reaction. The results, reported in Table V, indicate that catalysis and not ATP binding is rate-limiting for each of these enzymes.

TABLE V

Ratios of k_{obs} values measured for single-turnover reactions of E + [^{14}C]ATP → E-P · [^{14}C]AMP catalyzed by 40 μM and 80 μM wild-type, R219A, R219E, E434A/E437A, or T453A PPDK

Reaction contains 40 or 80 μM enzyme, 10 μM [^{14}C]ATP, 2.5 mM Co^{2+}, 10 mM NH_4^+ and 50 mM K^+Hepes (pH 7.0, 25 °C).

Enzymes	WT	R219A	R219E	DEDA	T435A
Ratio trial 1[a]	1.3	1.15	1.26	0.96	0.80
Ratio trial 2[a]		1.03	0.84	0.92	

[a] Ratio of the k_{obs} for the reaction containing 80 μM enzyme over the k_{obs} for the reaction containing 40 μM enzyme.

The k_{obs} values measured for the E·Mg(II) + [^{14}C]ATP + P_i → E-P·[^{14}C]AMP·PP_i·Mg(II) reaction catalyzed by the R219E, R219A, E434A/E437A, E271A, T453A, and S262W mutants (Table III) mirror (within error limits) the k_{obs} values measured for the E·Co(II) + [^{14}C]ATP → E-PP· [^{14}C]AMP·Co(II) reaction (Table IV). Thus, the first (E-PP·AMP forming) step is rate-limiting. The k_{obs} values, therefore, are less than or equal to the rate constants for the second step catalyzed in the mutants.

Altered Active Site Versus Altered Domain-Domain Docking in PPDK Mutants—The kinetic properties measured for the R219E, R219A, E434A/E437A, E271A, T453A, and S262W PPDK mutants show that the amino replacements made inhibit catalysis of the E + ATP → E-PP·AMP partial reaction. Because catalysis of this partial reaction depends both on the integrity of the N-terminal domain active site and on the accurate placement of the His^{455} residue into the active site, impaired catalysis in these mutants can derive from an alteration in the active site environment and/or an alteration in the domain-domain docking process. Here, we argue that the N-terminal domain active sites in the PPDK mutants[3] are intact and that impaired catalysis derives from altered domain-domain docking.

First, we note that the mutation sites are located at the surface of the N-terminal or central domains. We do not anticipate that the amino acid substitutions will alter the domain fold (as is demonstrated for the T453A mutant by x-ray crystallographic analysis; see below), and in this way inhibit catalysis of the E + ATP → E-PP·AMP partial reaction. Substitutions of Arg^{219}, Glu^{271}, Lys^{149}, and Glu^{434}/Glu^{437} involve changes in the electrostatic properties of the domain surface, not in but near the active site. In previous (unrelated) studies, analogous electrostatic perturbations have been generated at the N-terminal domain surface in close vicinity of the active site, without alteration of catalytic activity (in the Lys^{163},

[3] The exception may be the S262W mutant. This mutant displays a modest reduction in ATP binding affinity and large reduction in catalytic efficiency. We suspect that the large Trp side chain causes conformational changes effecting both the ATP binding site and the domain-domain binding site.

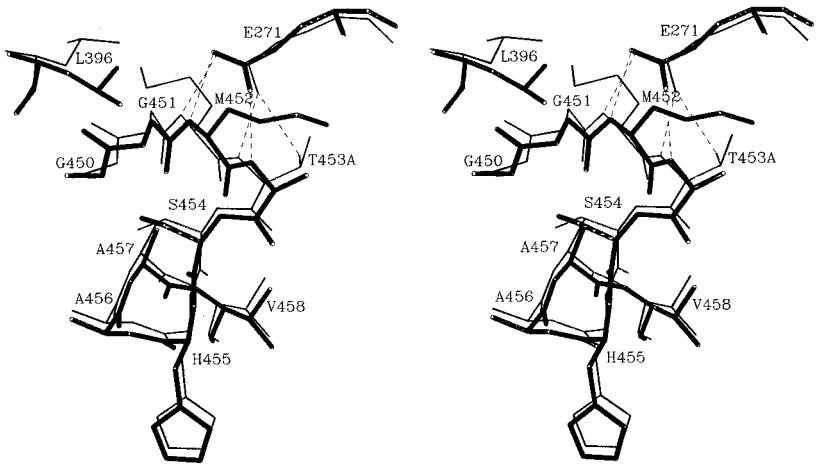

FIG. 7. **Superposition of the wild-type (*thin lines*) and T453A PPDK structures (*thick lines*) in the vicinity of the mutation site.** The electrostatic interactions between the carboxylate group of Glu^{271} and residues 452 and 453 are shown in *dashed lines* (the interaction with the hydroxyl group is eliminated in the mutant PPDK). The current model has a conventional *R*-factor of 0.177 and free R-factor of 0.294 for the 21,068 reflections between 20 and 2.65 Å resolution for which $F \geq 2\sigma(F)$ (R-factor = $\Sigma_{hkl} \| F_o| - |F_c| | / \Sigma_{hkl} |F_o|$,where F_o and F_c are the observed and calculated structure factors). The stereochemical parameters are well within the range known from crystal structures of small peptides. The root-mean-square deviations from ideal values for bond lengths and bond angles of the standard geometry as compiled by Engh and Huber (*19*) are 0.012 Å and 1.7°, respectively. The model includes 869 of the 874 amino acid residues (the N-terminal methionine and residues 506–509 are associated with regions of low electron density), 227 water molecules, and 2 sulfate ions. Within the accuracy of the structure determination, the overall structure is the same as that of the wild-type protein (2).

Lys^{177}, Glu^{168}, Glu^{170}, and Glu^{175} PPDK mutants examined) (5). Although it can be argued that these sites are not located at the domain-domain interface, we point out that two of the domain-domain interface residues examined in the present study, Ser^{262} and Lys^{149} have been replaced by an Ala residue without loss of catalytic activity.

Second, we note that mutation of Arg^{219} to Glu has the same impact on catalysis at active site 1 that mutation of Arg^{219} to Ala has. Thus, the loss of binding interaction between Arg^{219} and the Glu^{434}/Glu^{437} residues is what is critical to catalysis and not the type of charge alteration made at position 219. Moreover, which partner of the paired docking residues, Arg^{219} or Glu^{434}/Glu^{437}, is replaced in the mutagenesis experiment does not effect the outcome; the catalytic properties of the Glu^{434}/Glu^{437} mutant and the Arg^{219} mutant are similar.

Finally, we note that disruption of the Glu^{271}-Thr^{453}/Met^{452} docking site has more impact on catalysis than does disruption of the Arg^{219}-Glu^{434}/Glu^{437} docking site. Unlike the Arg^{219}-Glu^{434}/Glu^{437} docking site, the Glu^{271}-Thr^{453}/Met^{452} docking site is close to the His^{455} residue (see Fig. 3). The His^{455} side chain is positioned on the N terminus of a short helix, just down stream from the Glu^{271} docking residues Thr^{453} and Met^{452}. The backbone amide NHs of both of these residues as well as the side chain of the Thr^{453} residue bind with the Glu^{271} carboxylate group, thereby drawing the His^{455} into the active site region. Consequently, the Glu^{271}-Thr^{453}/Met^{452} docking site might play a more dominant role in the productive domain-domain binding than the Arg^{219}-Glu^{434}/Glu^{437} site, which is further removed from the His^{455}. Alternatively, the differential effects of mutating Arg^{219} and Glu^{271} may be attributed to the difference in the number of interdomain electrostatic interactions lost. Specifically, the present data indicate that the removal of a single interaction, regardless of the docking site involved, results in a $\sim 10^4$-fold reduction in k_{obs}. This may be a simple coincidence, or it may suggest that the contributions of the electrostatic interactions are additive, in which case one can rationalize the greater loss in activity for the E271A PPDK mutant in terms of the loss of three rather than one interaction.

Misalignment versus Decreased Residence Time by Impaired Domain-Domain Docking—Domain movement in PPDK occurs via bond rotation within the solvated linkers (Fig. 1). Domain-domain association occurs through the diffusion of the two tethered protein bodies through restricted solvent space. The binding equilibrium is controlled by the attraction between the two interfaced surfaces. Protein interfaces observed in protein dimers, protease-protein inhibitor complexes, and antibody-protein antigen complexes (where in permanent association is desired) range from 700 to 4900 $Å^2$ (16). In PPDK, for which the binding of between the two domain surfaces is intended to be transient, the accessible area buried in conformation 1 (Fig. 1) is $\sim$700 $Å^2$ (2).

TABLE VI
Statistics of x-ray crystallographic data collection for T453A PPDK

Space group	P_2
Cell parameters	a = 89.9 Å, b = 58.7 Å, c = 102.1 Å b = 95.2 °
Maximum resolution (Å)	2.6
No. of crystals used	1
No. of observations	43,302
No. of unique reflections	27,567
R_{merge}[a]	0.076
Completeness (%)	83 (68)[b]
$I/\sigma(I)$	11.7 (2.1)[b]

[a] $R_{merge} = \Sigma_{hkl}[(\Sigma_i|I_l - \langle I\rangle|)/\Sigma_i I_i]$.
[b] The values in the parentheses correspond to the highest resolution shell between 2.76 and 2.60 Å.

Hydrophobic interactions deriving from the desolvation of nonpolar residues are often present at protein-protein interfaces (17, 18). Inspection of the domain-domain interface within the PPDK structure reveals two matched sets of hydrophobic regions which may contribute to the intrinsic binding energy. The electrostatic interaction between Arg^{219} and Glu^{434}/Glu^{437} and between Glu^{271} and Thr^{453}/Met^{452}(NH) may also contribute to the domain-domain binding energy as well as provide specificity to the domain-domain interactions. A steering mechanism, based on the pairing of specific residues at the domain-domain interface, could reduce the number of collisions required to achieve productive binding of the catalytic His^{455} in the N-terminal domain active site.

Proof that the electrostatic interaction between Arg^{219} and Glu^{434}/Glu^{437} and between Glu^{271} and Thr^{453}/Met^{452}(NH) is used for domain-domain steering is not easily obtained. Crys-

tallization experiments of these mutant enzymes, which following structure determination would reveal if the relative orientation of the two domains has been altered, have been unsuccessful. Thus far, only the x-ray structure of the T453A mutant has been determined (see Fig. 7, Table VI, and "Experimental Procedures" for details). Within the accuracy of the structure determination, the overall structure is the same as that of the wild-type protein (2). The C_α atomic coordinates of the mutant and wild-type molecules superimpose with a root-mean-square deviation of 0.5 Å. The electron density map at the mutation site is consistent with the replacement of a threonine by an alanine residue at position 453. The interaction between the side chain of Glu^{271} and the hydroxyl group of Thr^{453} is therefore eliminated, but the remaining two interactions with the two NH groups of residues 452 and 453 are maintained (Fig. 7). In addition, the side chains of Met^{452} and Leu^{369} shift concertedly so that the Met^{452} side chain occupies space that was partially occupied in the wild-type protein by the methyl group of Thr^{453}, and the Leu^{396} side chain shifts toward the position occupied by Met^{452} in the wild-type protein. These changes are compensatory and therefore are not expected to impact significantly on the catalytic efficiency of the enzyme. Thus, although the structure of T453A PPDK provides evidence that the reduction in catalytic efficiency is *not* caused by alteration in active site conformation, it does not provide any indication of misalignment of the domain-domain surfaces. This static picture may or may not provide an accurate view of the dynamics between protein species in solution. The absence of a particular conformer in the crystal does not mean that it is also absent in solution.

CONCLUSIONS

The current model of PPDK catalysis involves the swivel-type movement of a central, phosphoryl carrier domain between the ATP/P_i active site of the N-terminal domain and the pyruvate active site of the C-terminal domain. We hypothesize that the stringently conserved residues at the respective domain-domain interfaces play an active role in guiding the catalytic His^{455} of the central domain into the active sites and holding it there long enough for catalysis to be completed. The loss of catalytic activity observed for the mutants examined in the present study supports the proposed roles of the N-terminal residues Arg^{219} and Glu^{271} in the productive binding of the central domain for catalysis of the ATP/P_i partial reaction.

REFERENCES

1. Wood, H. G., O'Brien, W. E., and Micheales, G. (1977) *Adv. Enzymol. Relat. Areas Mol. Biol.* **45,** 85–155
2. Herzberg, O., Chen, C. C., Kapadia, G., McGuire, M., Carroll, L. J., Noh, S. J., and Dunaway-Mariano, D. (1996) *Proc. Natl. Acad. Sci. U. S. A.* **93,** 2652–2657
3. Carroll, L. J., Mehl, A. F., and Dunaway-Mariano, D. (1989) *J. Am. Chem. Soc.* **111,** 5965–5967
4. McGuire, M., Huang, K., Kapadia, G., Herzberg, O., and Dunaway-Mariano, D. (1998) *Biochemistry* **37,** 13463–13474
5. McGuire, M., Carroll, L. J., Yankie, L., Thrall, S. H., Dunaway-Mariano, D., Herzberg, O., Jayaram, B., and Haley, B. H. (1996) *Biochemistry* **35,** 8544–8552
6. Xu, Y., Yankie, L., Shen, L., Jung, Y. S., Mariano, P. S., Dunaway-Mariano, D., and Martin, B. M. (1995) *Biochemistry* **34,** 2181–2187
7. Yankie, L., Xu, Y., and Dunaway-Mariano, D. (1995) *Biochemistry* **34,** 2188–2194
8. Mehl, A., Xu, Y., and Dunaway-Mariano, D. (1994) *Biochemistry* **33,** 1093–1102
9. Pocalyko, D. J., Carroll, L. J., Martin, B. M., Babbitt, P. C., and Dunaway-Mariano, D. (1990) *Biochemistry* **29,** 10757–10765
10. Wang, H. C., Ciskanik, L., Dunaway-Mariano, D., von der Saal, W., and Villafranca, J. J. (1988) *Biochemistry* **27,** 625–633
11. Cleland, W. W. (1979) *Methods Enzymol.* **63,** 500–513
12. Howard, A. J., Gilliland, G. L., Finzel, B. C., Poulos, T. L., Ohlendorf, D. H., and Salemme, F. R. (1987) *J. Appl. Crystallogr.* **20,** 383–387
13. Brunger, A. T. (1992) *X-PLOR Version 3.1: A System for X-ray Crystallography and NMR*, Yale University, New Haven, CT
14. Roussel, A., and Cambillu, C. (1989) *TURBO FRODO; Silicon Graphics Geometry Partner Directory*, Silicon Graphics, Mountain View, CA
15. Deleted in proof
16. Stites, W. E. (1997) *Chem. Rev.* **97,** 1233–1250
17. Privalov, P. L., and Gill, S. J. (1988) *Adv. Protein Chem.* **39,** 191–234
18. Spolar, R. S., Ha, J. H., and Record, M. T. (1989) *Proc. Natl. Acad. Sci. U. S. A.* **86,** 8382–8385
19. Engh, R. A., and Huber, R. (1991) *Acta Crystallogr. Sect. A* **47,** 392–400